Journal of Electrical Engineering, Vol. 75, No. 1, 2024, pp. 29-40

sciendo

PAPERS

# Design of a bidirectional EV charger using unit template-based current-controlled synchronous reference frame hysteresis

**Ambuli B. R. Etemesi[1], Tamer F. Megahed[1,2], Haruichi Kanaya[3], Diaa-Eldin A. Mansour[1,4,*]**

Existing distribution networks were not designed with large-scale electric vehicle (EV) charging infrastructure in mind. Integrating EV charging stations with the distribution grid might lead to power quality (PQ) issues at the point of common coupling (PCC). This work proposes a two-mode, unit template-based synchronous reference frame hysteresis current-controlled (SRF-HCC) three-phase Level 2 EV charger. Mode one focuses on charging the EV battery from the grid (G2V) and utilizes current and voltage control techniques to enhance battery life and performance. Whereas mode two enables the EV's stored energy to be discharged to the grid (V2G) by the EV user, allowing the sale of power to support the transient effect of the grid voltage and frequency and enhancing the grid's PQ. The HCC generates switching pulses for both the AC-DC and buck-boost converters. The SRF-based unit template-based control (SRF-UTC) method ensures system stability, voltage, and frequency regulation for power exchange with the grid by combining its efficiency with that of the HCC. The EV charger proposal comprises three primary components: a 3-phase bidirectional AC-DC converter, a bidirectional buck-boost converter, and a filter circuit. The proposed system was modeled using MATLAB/Simulink and evaluated in two case studies to assess its performance.

Keywords: electric vehicles, power quality, vehicles to grid, grid to vehicles, hysteresis control

## 1 Introduction

### 1.1 Motivation

Over the decades, the transport sector, one of the largest consumers of energy, has utilized fossil fuels to power internal combustion engine vehicles. This sector consumes up to one-fourth of the total energy and produces one-third of greenhouse gases compared to other economic players. Fossil fuels, when burnt, produce greenhouse gases that have far-reaching effects on the environment. The electrification of the transport sector has been considered a perfect medium for moving away from internal combustion engines to electric vehicles (EVs) because they are powered by batteries that are charged from the grid [1].

According to [2], the number of EVs by 2022 was 16.5 million up from 5.5 million in 2018 which signifies a tripling of the global number of EVs with the number poised to rise to about 130 million by 2030 and overall demand for electrical energy of 1100 Terawatt-hours. As the number of EVs rises, there is a need to invest in robust and appropriate charging infrastructure to alleviate range anxiety among users who would like to travel long distances. However, existing distribution networks were not constructed with large-scale charging infrastructure deployment in mind. As a result of incorporating charging stations into distribution networks, voltage profiles may degrade, harmonic distortions may occur, and peak load may increase [3].

### 1.2 Related works

These power quality (PQ) issues arise because of the interfacing converters used in the power transfer between EV battery and grid. Previous research has focused solely on one-way energy transmission, i.e., from the distribution grid to the EV's battery. Further, recent research has established grid-to-vehicle (G2V) and vehicle-to-grid (V2G) technology dual energy relaying between EVs and the distribution grid. EV batteries are charged during off-peak times, and during peak load times, the energy stored in the EVs is discharged into the distribution grid. Furthermore, the dual energy relaying V2G technique's additional advantages have made it to be embraced in the scientific and engineering communities. Depending on the item engaging with the EV, the V2G approach can be applied to vehicle-to-home, vehicle-to-vehicle, and vehicle-to-

[1] Electrical Power Engineering Department, Faculty of Engineering,
Egypt-Japan University of Science and Technology (E-JUST), New Borg El Arab City, Alexandria 21934, Egypt
[2] Electrical Engineering Department, Mansoura University, El-Mansoura 35516, Egypt
[3] Faculty of Information Science and Electrical Engineering, Kyushu University, Fukuoka, Japan
[4] Electrical Power and Machines Engineering Department, Faculty of Engineering, Tanta University, Tanta 31511, Egypt
* diaa.mansour@ejust.edu.eg

https://doi.org/10.2478/jee-2024-0005, Print (till 2015) ISSN 1335-3632, On-line ISSN 1339-309X

building scenarios. The batteries of the EVs are used to give power in all these scenarios [4, 5].

The CHAdeMO charger standard currently supports bidirectional power transfer from the EV battery pack to the grid [6]. Furthermore, the Society of Automotive Engineers (SAE J1772) describes standards for EV chargers with different power levels, as in [7]. The standard describes the EV charger levels, power supply, location, implementation site, and maximum power and current. Level 1 charger is slow and is suitable for overnight charging whereas the level 2 charger is a moderately fast charger, and for fast charging, utilization of level 3 and DC chargers is necessitated. The level of charging is selected depending on the EV user's preference and available power supply.

To achieve effective incorporation of EVs into the distribution grid, properly controlled grid-interfaced power electronic converter-based charging stations are crucial. They play a critical role in V2G and G2V operations. In this scenario, any EV charger control technique should be capable of significantly reducing ripples in DC voltage and current, keeping harmonic alteration at standardized level, and enhancing PQ on both the AC and DC sides. So, the EV charger must operate in multiple modes under quickly evolving operating conditions necessitating the need to have a quick-response controller that can adjust to the prevailing conditions [8].

A classical synchronous reference frame-phase locked loop (SRF-PLL) technique is adopted in [9,10] to control the voltage source converter (VSC). According to [11], Adaline-based control and instantaneous reactive power theory are not as effective as the SRF theory-based control method, which is unambiguous, simple, and adaptable. According to [12–14] UTC is an easy and competent control approach for converters. Further, the hysteresis controller (HC) demonstrates healthier total harmonic alteration than the proportional-integral (PI) controller because of its fast response current loop but has low order harmonics and can be implemented with minimum hardware despite its variation in switching frequency [15,16].

### 1.3 Contribution

In this work, a two-mode, unit template-based synchronous reference frame hysteresis current-controlled (SRF-HCC) three-phase Level 2 EV charger is designed. The first mode focuses on charging the EV battery from the grid (G2V). Current and voltage control techniques are employed to enhance battery life and performance. The HCC generates switching pulses for both the AC-DC and buck-boost converters.

In the second mode, the EV user can discharge the stored energy to the grid (V2G), allowing the sale of power during peak hours without affecting the grid's PQ. Moreover, this mode can also support the grid's voltage and frequency transient changes. This mode utilizes the SRF-based unit template-based control (SRF-UTC) method. The SRF-UTC method ensures system performance, stability, voltage regulation, and frequency regulation for power exchange with the grid. In this operating mode, discharge current is controlled while considering the state of charge (SOC) of the EV battery and accommodating the EV user's preference. The SOC must be within acceptable limits to prevent deep discharge, and participants in the V2G program receive lower charging rates as an incentive.

Overall, the proposed control methodology combines the efficient and simple SRF-UTC approach with the HC to achieve reliable and effective converter operation in both charging and discharging modes. Furthermore, the proposed control strategy exhibits a fast dynamic response, is simple to implement, includes maximum current limiting, enhances system robustness, and requires minimal hardware.

The main contributions of this work can be summarized as follows:

1. Design of a two-mode, unit template-based SRF-HCC EV charger, enabling efficient and flexible charging functionality.
2. First mode focuses on efficient EV battery charging from the grid (G2V).
3. HCC generates switching pulses for AC-DC and buck-boost converters.
4. Second mode enables EV users to sell stored energy to the grid (V2G) during peak hours or to support the grid voltage.
5. Utilizes SRF-UTC method for stable and regulated power exchange with the grid.

### 1.4 Structure

This paper is segmented as follows. Section 2 covers the proposed system block diagram. In Section 3, the proposed control algorithms are discussed. In Section 4, the simulation results are presented. Section 5 compares the proposed design result with published works. Finally, Section 6 concludes the paper and outlines future works.

## 2 Proposed system

Shown in Fig. 1 is a detailed structure of the three-phase EV charger. The charger is interfaced to the grid through two power conversion stages, with galvanic isolation via an electrolytic capacitor. Stage one is the AC-DC conversion, tailed by the DC-DC conversion. To achieve this, the three-phase charger utilizes six ideal insulated-gate bipolar transistors (IGBTs) for the

AC-DC converter and two ideal metal-oxide-semiconductor field-effect transistors (MOSFETs) switches for the buck-boost converter. The charger operates in two distinct modes: G2V and V2G. In the G2V mode, the charger converts the grid's AC voltage into DC through an AC-DC rectifier, operating at a unity power factor while producing a sinusoidal current. Subsequently, a DC-DC buck conversion takes place to charge the EV battery. In the V2G mode, the AC-DC converter acts as an inverter, while the DC-DC converter functions in boost mode. In this configuration, power is supplied to the grid, causing the inverter to operate as a controlled current source.

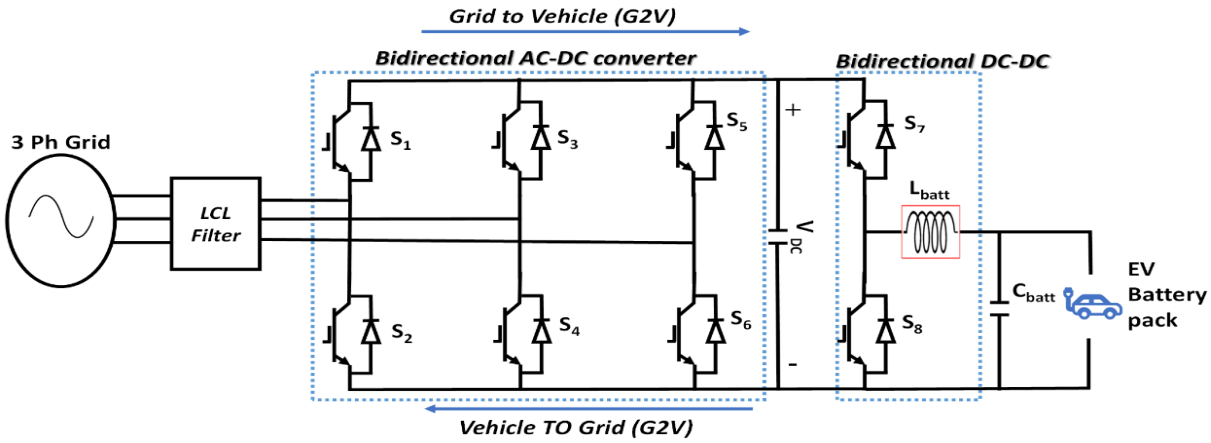


**Fig. 1.** Three-phase bi-directional charger

The AC-DC converter is the front-end converter which is connected to the grid via a filter. A higher-order inductor-capacitor-inductor (LCL) filter is used in this work because of the strict grid standards and codes that necessitate attenuation of high-frequency signals/harmonics due to the high switching frequencies from the IGBTs. The LCL filter components are designed as per the criteria used in [16, 17].

This converter's DC link capacitor is designed to ensure that the converter operates effectively in the G2V and V2G modes. For easy controlling and effective power transfer during transient, the peak point voltage of the PCC should be above the DC-link voltage as

$$V_{DC} = a\sqrt{2}\, V_L. \quad (1)$$

The DC bus capacitance is designed to curb its voltage ripple to be below five percent of the least DC bus voltage [18-19]. The DC bus capacitance is then calculated as

$$C_{DC} = \frac{P_{DC}}{V_{DC} 4\pi f \Delta V_{DC}}, \quad (2)$$

where $V_{DC}$ is the DC-bus voltage, $V_L$ is the line voltage, $P_{DC}$ is the maximum DC power, $f$ is the grid frequency, $\Delta V_{DC}$ is the allowable ripple in the $V_{DC}$ selected as 1.5%, and $a$ is the overload factor 1.1.

## 3 Proposed controller

Grid-connected EV chargers are required to operate with unity power factor (UPC) operation to achieve the recommended power quality standards as given in the IEC-61000 and IEEE 519-1992 (revised in 2014) [20-22]. A grid-connected EV charging station's performance is determined by the control method used to guarantee smooth working plus retrieval of the grid reference currents. Specific restrictions, such as harmonics, must be addressed by control algorithms of the grid-connected converters.

### 3.1 Voltage source converter algorithm

In this system, which should have solely sinusoidal currents, the voltage source converter (VSC) functions as an active power filter (APF) to generate a harmonic current that is the same as and opposing to the direction of the grid current. Unit template control (UTC) system, a time-domain system, is employed in this work to synchronise the converter with the voltage of the grid by extracting unit template (UT) and removal of harmonics [12-14].

The active and reactive/quadrature power ($i_d$ and $i_q$) components are generated as shown in Fig. 2. The proposed VSC control algorithm comprises four loops, which are described as follows:

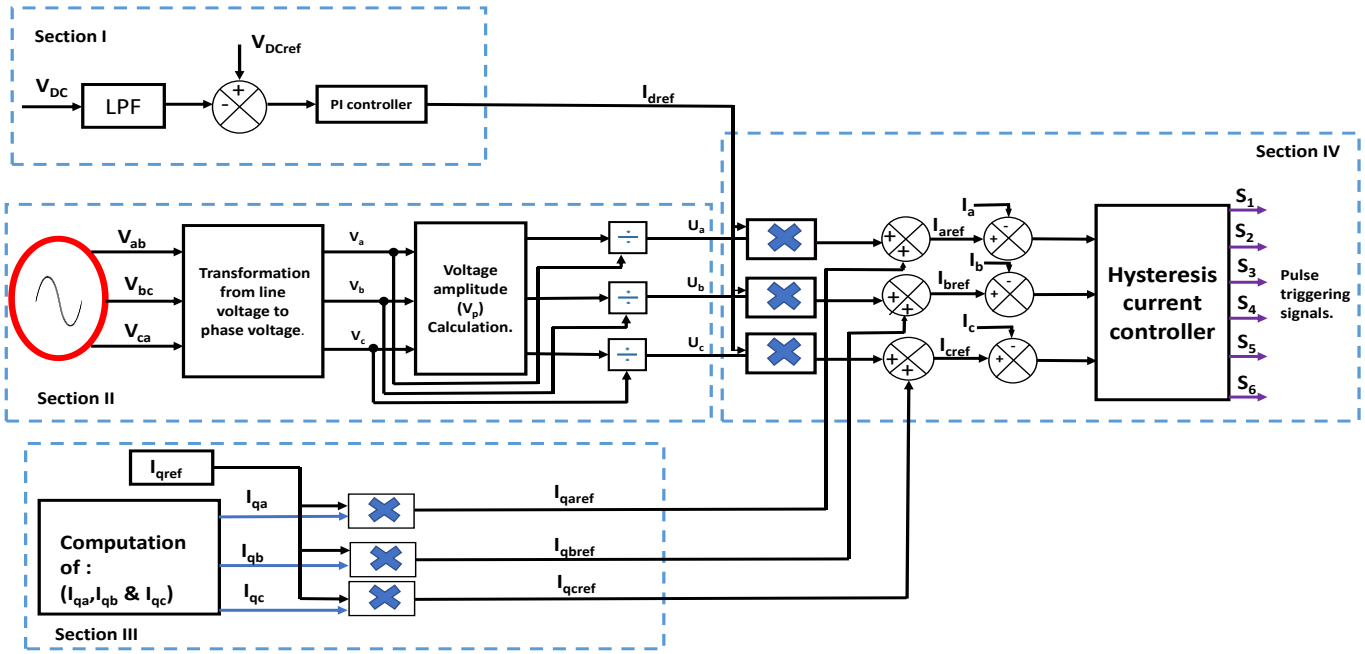


**Fig. 2.** Proposed voltage source converter control scheme

**Section I:** The sensed DC bus voltage ($V_{DC}$) is first sent through a low pass filter (LPF) for filtration. The error to be sent to the PI controller to generate the overall active power component ($I_{dref}$) as shown in Eqn. (3) is produced by comparing the sensed $V_{DC}$ to the reference DC voltage ($V_{DCref}$).

$$I_{dref} = K_p\left(V_{DCref} - V_{DC}\right) + \int K_i\left(V_{DCref} - V_{DC}\right) dt \tag{3}$$

**Section II:** The point of common coupling (PCC) grid line voltage ($V_{ab}$, $V_{bc}$ and $V_{ac}$) and grid current ($I_a$, $I_b$ and $I_c$) are measured. Grid per phase voltages ($V_a$, $V_b$ and $V_c$) are calculated from the line voltages using Eqn. (4) then passed through band pass filter to eliminate any noise in them and subsequently used to calculate the amplitude of the voltage ($V_p$) at the PCC using Eqn. (5). In-phase UT ($u_a$, $u_b$ and $u_c$) are also calculated from the phase voltage using Eqn. (6). Relatedly the quadrature in-phase UT ($q_a$,$q_b$ and $q_c$) are also calculated using Eqn. (7).

$$\left.\begin{aligned} V_a &= \frac{2}{3}V_{ab} + \frac{1}{3}V_{bc} \\ V_b &= \frac{1}{3}V_{ab} + \frac{1}{3}V_{bc} \\ V_c &= -\frac{1}{3}V_{ab} - \frac{2}{3}V_{bc} \end{aligned}\right\} \tag{4}$$

$$V_p = \sqrt{\frac{2}{3}\left(V_a^2 + V_b^2 + V_c^2\right)} \tag{5}$$

$$u_a = \frac{V_a}{V_p}, \quad u_b = \frac{V_b}{V_p}, \quad u_c = \frac{V_c}{V_p} \tag{6}$$

$$\left.\begin{aligned} q_a &= -\frac{u_a}{\sqrt{3}} + \frac{u_c}{\sqrt{3}} \\ q_b &= \sqrt{3}\frac{u_a}{2} + \frac{(u_b - u_c)}{2\sqrt{3}} \\ q_c &= -\sqrt{3}\frac{u_a}{2} + \frac{(u_b - u_c)}{2\sqrt{3}} \end{aligned}\right\} \tag{7}$$

**Section III:** Here the quadrature reference currents ($I_{qaref}$, $I_{qbref}$ and $I_{qcref}$) are calculated by multiplying the quadrature unit templates from Eqns. (7) with the reference power reactive component ($I_{qref}$) shown in Eqns. (8).

$$\left.\begin{aligned} I_{daref} &= I_{dref} \times q_a \\ I_{dbref} &= I_{dref} \times q_b \\ I_{dcref} &= I_{dref} \times q_c \end{aligned}\right\} \tag{8}$$

**Section IV:** A product of the in-phase UT ($u_a$, $u_b$ and $u_c$) generated in section II and the overall active power component ($I_{dref}$) is utilised to calculate active power reference values ($I_{daref}$, $I_{dbref}$ and $I_{dcref}$) as shown in Eqns. (9). Following that, active current and reactive

data is summed to give the reference grid currents as illustrated in Eqns. (10).

$$\left.\begin{aligned} I_{daref} &= I_{dref} \times u_a \\ I_{dbref} &= I_{dref} \times u_b \\ I_{dcref} &= I_{dref} \times u_c \end{aligned}\right\} \quad (9)$$

$$\left.\begin{aligned} I_{aref} &= I_{daref} + I_{qaref} \\ I_{bref} &= I_{dbref} + I_{qbref} \\ I_{cref} &= I_{dcref} + I_{qref} \end{aligned}\right\} \quad (10)$$

VSC pulse triggering signals are produced by the HCC by ensuring that the current error between the measured grid currents $I_a$, $I_b$ and $I_c$ and the generated reference current generated in Eqns. (10) is confined in a hysteresis band $h$ as shown in Fig. 3. HCC is a switching logic-based controller. $S_1$ and $S_2$ are complementary switches. When $I_a > I_{aref} + h$, $S_1$ opens and $S_2$ closes. Similarly, when $I_a < I_{aref} - h$, $S_1$ closes and $S_2$ opens. The switching logic for the other two phases is generated in the same manner as the first phases.

The proposed approach is useful in suppressing harmonics by mathematical processes, resulting in balanced grid currents. Because the extraction of reference currents $I_{aref}$, $I_{bref}$ and $I_{cref}$ is computationally easier and takes a short time compared to the PLL (Phase-Locked Loop) system.

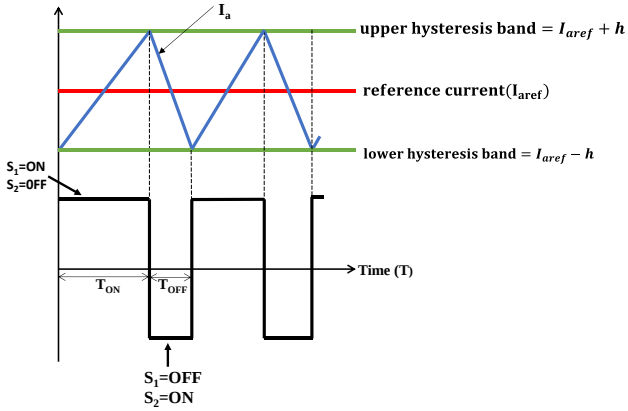


**Fig. 3** Hysteresis current controller switching scheme

### 3.2 Control algorithm for the bidirectional DC-DC converter

This converter is used to manage the power exchange between the electric grid and EV. It enables the EV to charge from the grid in G2V mode and supply power to the grid in V2G mode.

The battery charging control working of a DC-DC converter is illustrated in Fig. 4, which has two operational modes: charging and discharging. The buck operation shown in Fig. 5a. is the charging mode. On the other hand, Fig. 5b shows the boost operation when the EV is in discharge mode.

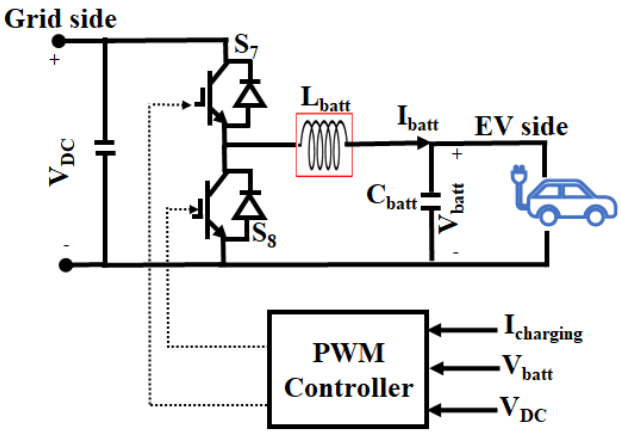


**Fig. 4** Bi-directional DC-DC converter

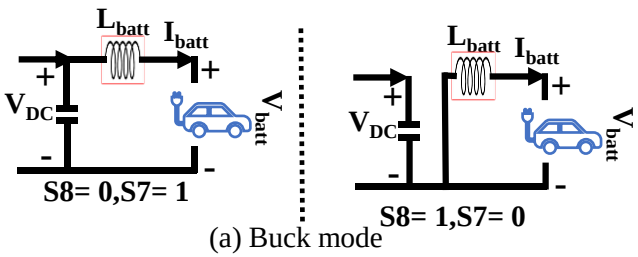


(a) Buck mode

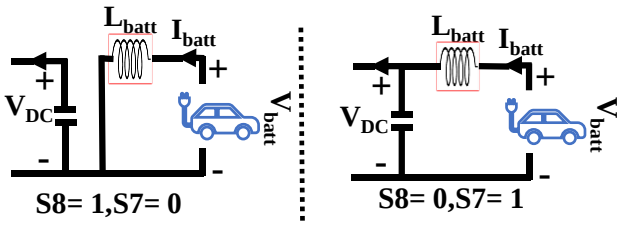


(b) Boost mode

**Fig. 5.** Buck & boost mode operation topologies

The bidirectional DC-DC converter operation involves controlling both the input and output side voltage and current levels. This is achieved through a control algorithm as described in Fig. 6 that adjusts the duty cycle of the converter's switching elements $S_7$ and $S_8$. The control algorithm ensures that the converter operates in a stable and efficient manner, while also meeting the constraints of the grid and the EV battery.

The control algorithm handles the dual operating mode of current control (CC) and voltage control (VC) during the charging mode, as well as V2G operation. There are three operation modes described as follows:

- The VC recharging mode involves an outer control loop that regulates battery voltage ($V_{batt}$) to a reference value ($V_{batt\_ref}$). This loop generates a reference signal for the charging current ($I_{batt\_1}$) flowing through the inductor. The deviation between the measured battery current ($I_{batt}$) and $I_{batt\_1}$ is then fed into the inner current control loop, which calculates the feed-forward term of the duty cycle ($D_{FF}$) for the DC-DC converter. It is worth noting that the feedback term of the duty cycle ($D_{FB}$) is a portion of the overall duty cycle (D). The feed-forward term ($D_{FF}$) is added to enhance the converter's start-up behaviour.
- CC charging mode: only the inner current loop is used to control $I_{batt}$ to the battery reference value ($I_{batt\_ref}$).
- V2G mode: only the inner current loop is used to discharge the EV battery following the reference value.

Table 1 presents the buck-boost formulation, which includes $L_{batt}$ as the battery filter for minimizing current ripple, $V_{batt}$ as the battery voltage, $V_{DC}$ as the DC bus voltage, $I_{batt}$ as the battery output current, $I_{batt\_1}$ as the inductor current, $F_{sw}$ as the switching frequency of the DC-DC converter, and $D$ as the duty cycle [23].

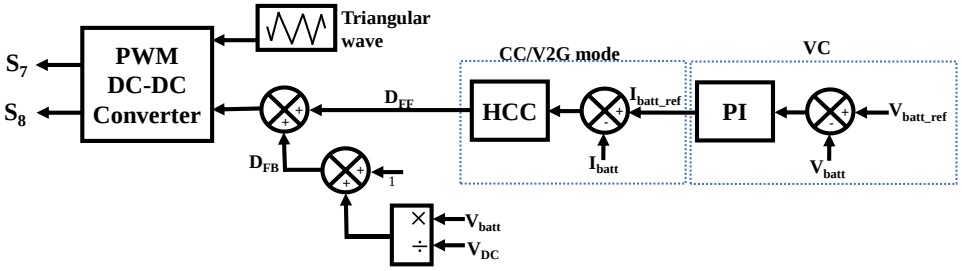


**Fig. 6.** PWM control scheme

**Table 1.** Buck-Boost operation modes

| Term | Buck | Boost |
|---|---|---|
| Duty cycle | $D = \frac{V_{batt}}{V_{DC}} = \frac{T_{on}}{T}$ | $D = 1 - \frac{V_{DC}}{V_{batt}}$ |
| Inductance | $L_{batt} = \frac{V_{batt}(1-D)}{F_{sw} * \Delta I_{batt}}$ | $L_{batt} = \frac{V_{batt} * D}{F_{sw} * \Delta I_{batt}}$ |
| Maximum output current | $I_{battmax} = I_{batt} - \frac{\Delta I_{batt}}{2}$ | $I_{battmax} = L_{B-min}\frac{\Delta I_B}{2}(1-D)$ |
| Maximum switching current | $I = I_{batt} + \frac{\Delta I_{battmax}}{2}$ | $I = \frac{I_{batt}}{1-D} + \frac{\Delta I_{battmax}}{2}$ |

### 3.3 Operation framework

Illustrated in Fig. 7 is the flowchart that outlines the operation methodology of the charger, which comprises two modes: V2G and G2V. The EV user has the liberty to choose their preferred mode. In the G2V mode, the EV battery parameters such as $V_{batt}$, battery temperature, SOC and $I_{batt}$ are detected and the EV battery charges at CC if $V_{batt}$ is less than the maximum battery voltage ($V_{battmax}$) by adjusting the buck duty cycle ($D_{\text{buck}}$) to maintain a constant charging current. When the $V_{batt}$ becomes equal to $V_{battmax}$ the charging shifts to CV mode by adjusting the $D_{\text{buck}}$ to maintain the charging voltage at $V_{battmax}$ while the charging current is reduced exponentially. When $I_{batt}$ reaches a preset current ($I_{preset}$), the charging stops because the EV battery is fully charged and disconnected from the source to prevent overcharging and battery damage.

In the V2G mode, if there is no problem with the grid, the EV battery chargers as described in the G2V mode. On the contrary, the V2G strategy provides grid services, such as power supply reserve and grid regulation. EVs act as a spinning reserve or storage system, injecting power into the grid to maintain the balance between demand and supply. This is achieved through a large scale of EVs, as individual vehicles' small battery capacity cannot make a significant impact. The V2G strategy also helps regulate grid frequency and voltage by charging or discharging EV batteries to raise or lessen the load demand, maintaining the frequency near the nominal value. Additionally, EVs can inject reactive power into the electric grid, compensating for voltage drops caused by system losses and load demand, thereby aiding in voltage regulation. To participate in V2G, EV user's preference is considered with an incentive of lower EV charging price.

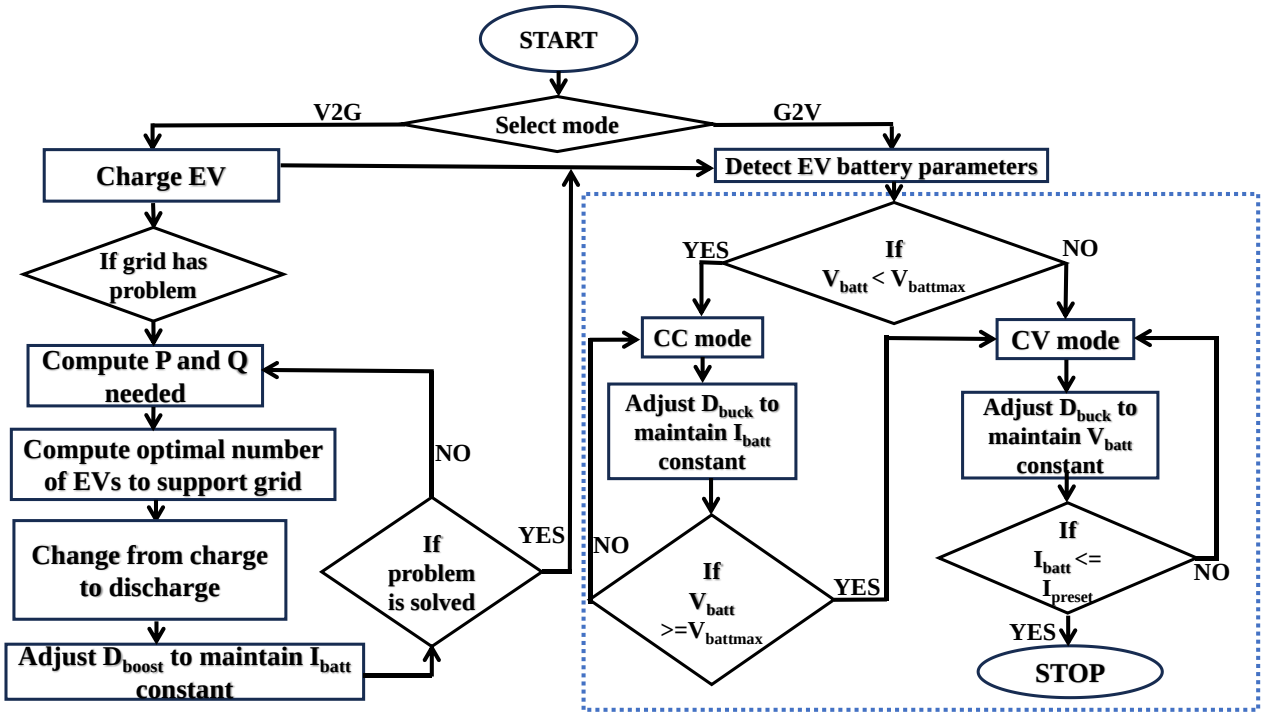


**Fig. 7.** Flow chart for G2V and V2G charging processes

## 4 Results and discussion

The system's performance is assessed using a simulation study performed in the MATLAB/Simulink software with the system requirements and passive components values as stated in Table 2. Aside from that, a lithium-ion battery with a 360 V nominal voltage and capacity 150 Ah is used for charge and discharge reasons. Different parameters, such as the grid voltage $V_g$, grid current $I_g$, battery current $I_{batt}$, $V_{batt}$, $V_{DC}$, SOC, power factor (PF), $I_g$ total harmonic distortion, and converter active and reactive power, are assessed for the proposed system working in two modes of operation. Two case studies were used to simulated and assess the system. The first case system is simulated for 4 seconds with a G2V and V2G current of 30 A, where the first 2 seconds in G2V and the second 2 seconds in V2G show a sudden shift from the G2V to the V2G mode. In the second case study, the system is simulated for 14 seconds. The G2V and V2G battery currents are reduced gradually in steps of 10 A after every 2 seconds, and the

power taken from the grid or discharged to the grid is observed with the different current levels. Comprehensive performance of both modes under the two case studies is reviewed in the subsections that follow.

**Table 2.** System requirements and passive components values

| Parameter | Value |
|---|---|
| $V_{grid}$ | 400 V (L-L) |
| Grid frequency ($f$) | 50 Hz |
| Grid ($L_{grid}$) and inverter side inductor ($L_{inv}$) | 1 mH and 3 mH |
| Filter capacitor | 10 µF |
| Battery pack side capacitor ($C_{batt}$) | 30 µF |
| Maximum switching frequency ($f_{sw}$) | 12,000 Hz |
| Gains for PI control | $K_p$=1.3, $K_i$=100 |

## 4.1 Performance during G2V

### *4.1.1 Case one*

In G2V mode, grid together with bidirectional battery side converters are utilized to charge the EV battery pack from grid. $I_g$ and $V_g$ are supposed to be sinusoidal in this mode, with a near unity power factor with $I_{batt}$ maintained at a constant. $I_g$ is shown to be in phase with the $V_g$ as shown in Fig. 8.

In Fig. 9, the drawn active and reactive powers are just about the rated power of 15 kW and zero, respectively, which shows that the PF is one. Whereas Fig. 10, a total harmonic distortion (THD) of 0.28% present in $I_g$ is within the IEEE standard 519, demonstrating the control converter is effective for the rectification process**.**

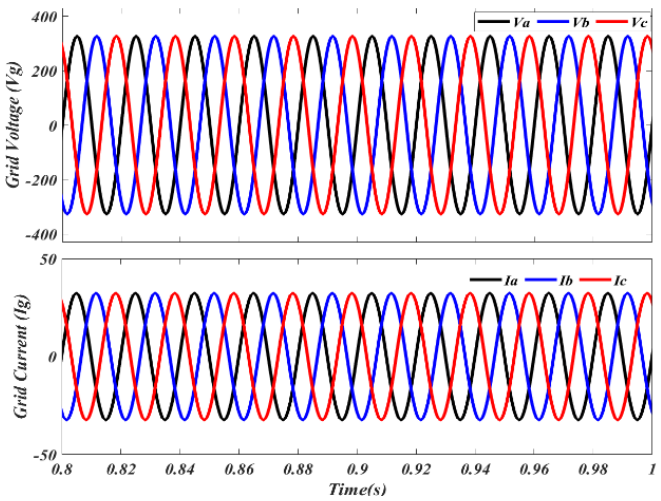


**Fig. 8.** $V_g$ and $I_g$ in G2V mode for cases one and two

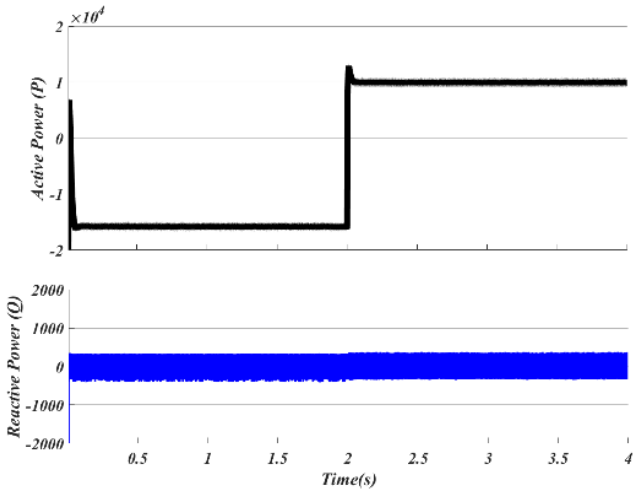


**Fig. 9.** Drawn active and reactive power in G2V and V2G modes for case one

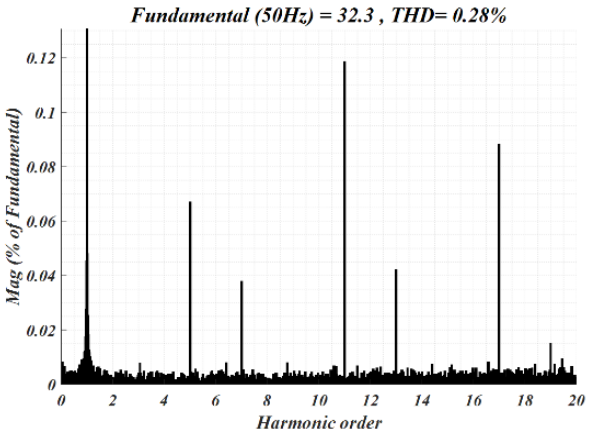


**Fig. 10.** Grid current THD in G2V mode case one

From $t$=0 s to $t$=2 s (charging mode) as in Fig. 11, the performance of the EV battery is provided in terms of SOC, $V_{batt}$ and $I_{batt.}$ An increase in SOC and a negative value of $I_{batt}$ are seen, and $V_{batt}$ increasing slightly above the norminal voltage of 360 V.

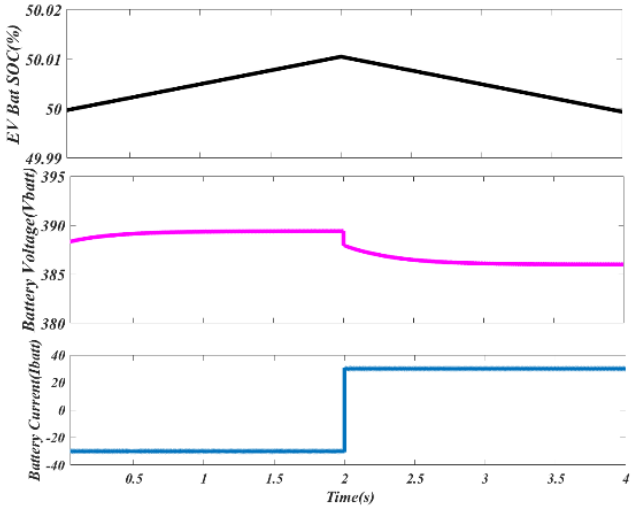


**Fig. 11.** SOC, battery voltage and current for case one

The performance of the $V_{DC}$ bus in G2V mode is shown in Fig. 12 from $t$=0 s to $t$=2 s. The resulting $V_{DC}$ bus is fed into the buck-boost converter, which uses buck mode control to charge the EV battery.

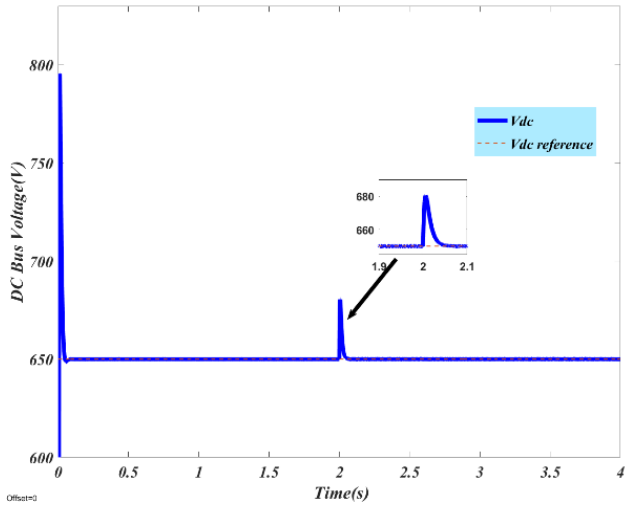


**Fig. 12.** DC bus voltage case study one

*4.1.2 Case study two*

The charging current gradually decreases from 30 A to zero in steps of 10 A after every 2 seconds until $t$=6 s. The $V_g$ and $I_g$ are observed to be sinusoidal and in phase, as shown in Fig. 8. As depicted in Fig. 13, the active power drawn decreases as the charging current reduces. However, the reactive power remains at zero, indicating that the charger is charging the EV battery pack at a unity power factor. The $I_g$ THD is as in Fig. 16 which is within the recommended IEEE 519 limits.

During the charging period, SOC,$V_{batt}$ and $I_{batt}$ are used to evaluate the working of the EV battery pack. These performance parameters are illustrated in Fig. 14 with the G2V mode section demonstrating the increase in SOC and a negative value of $I_{batt}$. It is concluded that a higher charging current results in a faster charging rate, while a zero current draw by the EV battery pack keeps the SOC constant.

The performance of the $V_{DC}$ bus is shown in Fig. 15, which is fed into the buck-boost converter. The converter employs buck mode control to charge the EV battery pack. The controller quickly tracks DC reference voltage, as evidenced by a variation of approximately 7.5 V during the charging and discharging current transitions in both G2V and V2G modes.

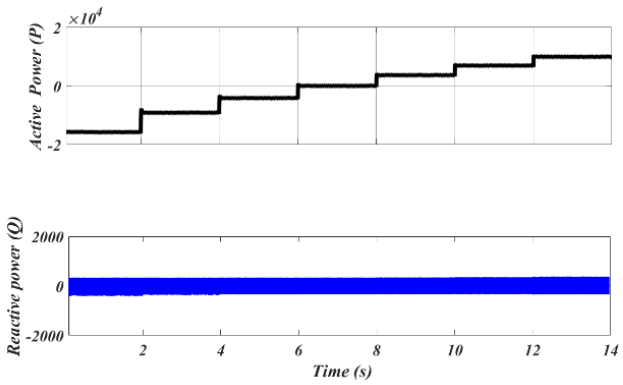


**Fig. 13.** Case study two G2V and V2G active and reactive power

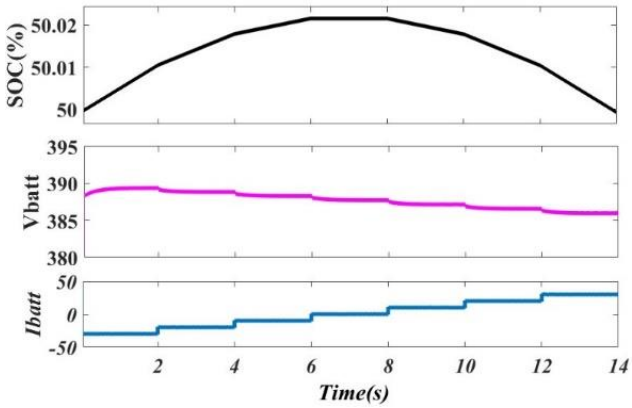


**Fig. 14.** Case study two SOC, battery voltage and currents

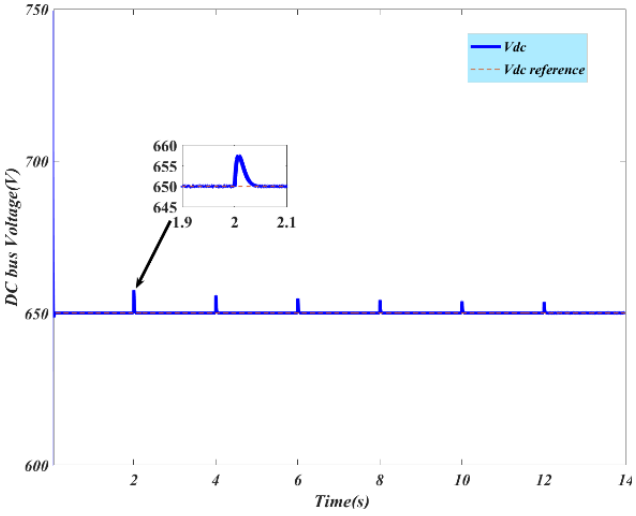


**Fig. 15.** DC bus voltage response for case two

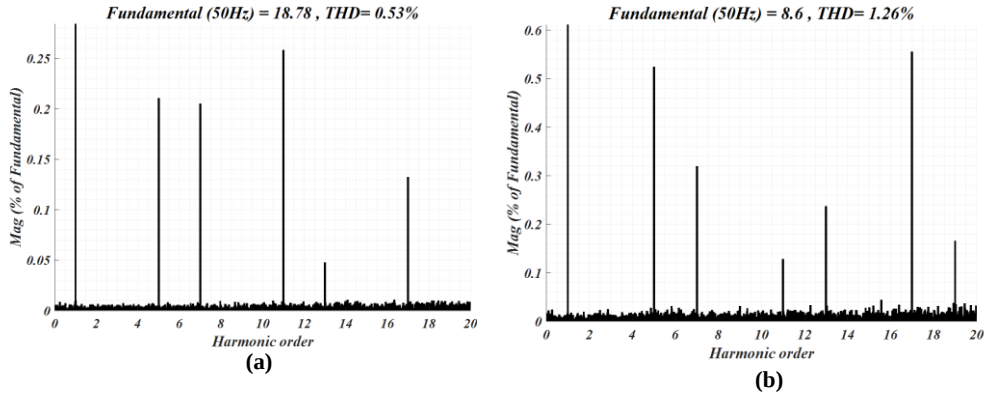


**Fig. 16.** THD for G2V mode: (a) charging at 20 A, (b) charging at 10 A

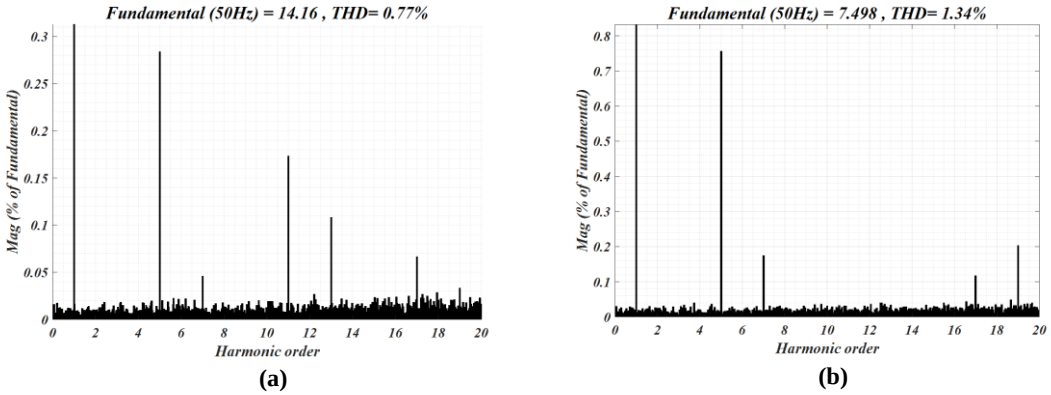


**Fig. 17.** THD in V2G mode: (a) discharging at 20 A, (b) discharging at 10 A

## 4.2 V2G / discharging mode

### *4.2.1 Case study one*

Power is sent to the grid from the EV battery pack in V2G. The DC bus has a greater voltage level than $V_{batt}$, therefore the buck-boost converter functions in boost mode. Depiction of the performance of the $V_{DC}$ bus is in Fig. 12 from $t$=2 s to $t$=4 s. The ripple in the $V_{DC}$ is due to the sudden change in the direction of flow of battery current, which finally settles at its 650 V reference in 0.001 s. Figure 11 shows the performance of the EV battery using the SOC, $V_{batt}$ and $I_{batt.}$ V2G mode section for $t$=2 s to $t$=4 s, where a positive current and a negative gradient of SOC indicates discharging. The grid receives DC power using the inversion mode. The $V_g$ and $I_g$ waveforms are seen in Fig. 18.

As illustrated in Fig. 19 the inverter control approach achieves the desired THD according to IEEE standard 519. Figure 9 shows that the built bidirectional unit template hysteresis charging infrastructure has accomplished the intended transfer of active and reactive powers, respectively.

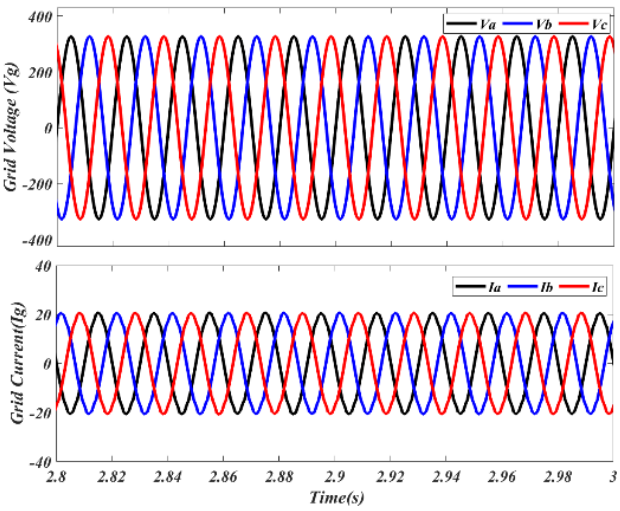


**Fig. 18.** Grid voltage and current in V2G mode for cases one and two

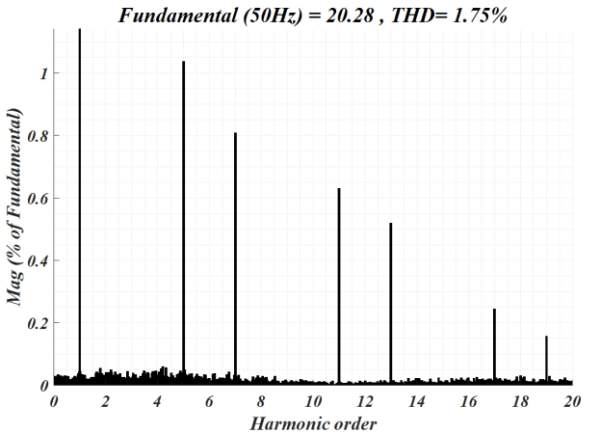


**Fig. 19.** THD in input current during V2G case one

*4.2.2 Case two*

The discharging current gradually increased from 0 A to 30 A in steps of 10 A, while $V_g$ and $I_g$ are observed to be sinusoidal and out of phase, as shown in Fig. 18. As depicted in Fig. 13, the active power injected into the grid increases as the charging current increases. However, the reactive power remains at zero, indicating that the charger is supplying power to the grid at a unity power factor. The $I_g$ THD is shown in Fig. 17.

During the V2G mode, the EV battery pack is evaluated using its SOC, $I_{batt}$, and $V_{batt}$. These performance parameters are illustrated in Fig. 14, with the V2G mode section demonstrating the reduction in SOC and a positive value of $I_{batt}$ during discharging. It is concluded that a higher discharging current results in a faster discharging rate, while a zero current draw by the EV battery pack keeps the SOC constant.

## 5 Comparison with other works

Table 3 compares the proposed charger's performance to some existing EV battery pack charging systems based on $I_g$ THDs. In [21], a three-phase uncontrolled diode charger is designed whose equivalent circuit parameters are estimated by a measurement-based method. Whereas [22] proposes and simulates a unipolar common DC bus and common AC Bus architecture for EV fast charging stations whose impacts on PQ are analysed. Lastly, in [18], a distribution grid power quality improved bidirectional EV charging station has been created, analysed, and integrated with a robust controller based DSTATCOM. From the results, it is obvious that the proposed method using unit template-based SRF with HCC kept the $I_g$ THD below the acceptable limits of 5%, which is the IEEE-519 THD standard.

**Table 3.** Comparison with other works

| EV Charging system | Power electronics device configuration | $I_g$ THD (%) | |
|---|---|---|---|
| | | G2V | V2G |
| [24] | 3-phase diode rectifier | 30 | - |
| [22] | 3-phase bidirectional converter | 1.12 | - |
| [18] | 3-phase bidirectional converter | 4.44 | 4.65 |
| Proposed system | 3-phase bidirectional converter with UTC | 0.28 | 1.75 |

## 6 Conclusion and future works

This study proposed, developed, and evaluated a two-mode, unit template-based SRF-HCC three-phase Level 2 EV charger. The proposed EV battery pack charger was subjected to a simulation study for G2V and V2G modes in two case studies under different charging/discharging currents. The charger's quality has been increased by controlling the bidirectional voltage source converter with a unit template-based synchronous reference frame control using an HCC. The PI controller efficiently manages the $V_{DC}$ bus to produce the *d-axis* component. The simulation study results show that the controller performs well in both $V_{DC}$ bus regulation and $I_g$ THD cutback. The THD for case studies one and two in the G2V operation mode is 0.28%, 0.53% and 1.26% whereas the THD in the V2G mode for both case studies is 1.75%, 0.77% and 1.34% respectively. Furthermore, the CC-CV control system reliably protects the EV battery pack from overcharging and severe draining. As a result, the proposed design will increase the EV charging infrastructure numbers. Future work will include the development of an experimental implementation of the proposed model with reactive power support.

## References


[1] S. Wang, J. Li, X. Liu, E. Zhao, and N. Eghbalian, "Multi-level charging stations for electric vehicles by considering ancillary generating and storage units," *Energy*, vol. 247, May 2022, doi: 10.1016/j.energy.2022.123401.

[2] International Energy Agency (IEA), "Global EV Outlook 2022 - Securing supplies for an electric future," 2022. [Online]. Available: https://www.iea.org/reports/global-ev-outlook-2022%0Ahttps://iea.blob.core.windows.net/assets/ad8fb04c-4f75-42fc-973a-6e54c8a4449a/GlobalElectricVehicleOutlook2022.pdf

[3] M. M. H. Khan *et al.*, "Integration of large-scale electric vehicles into utility grid: An efficient approach for impact analysis and power quality assessment," *Sustainability (Switzerland)*, vol. 13, no. 19, Oct. 2021, doi: 10.3390/su131910943.

[4] S. S. Ravi and M. Aziz, "Utilization of Electric Vehicles for Vehicle-to-Grid Services: Progress and Perspectives," *Energies*, vol. 15, no. 2. MDPI, Jan. 01, 2022, doi: 10.3390/en15020589.

[5] M. Lu, O. Abedinia, M. Bagheri, N. Ghadimi, M. Shafie-Khah, and J. P. S. Catalão, "Smart load scheduling strategy utilising optimal charging of electric vehicles in power grids based on an optimisation algorithm," *IET Smart Grid*, vol. 3, no. 6, pp. 914-923, Dec. 2020, doi: 10.1049/iet-stg.2019.0334.

[6] CHAdeMO, "CHAdeMO." Accessed: Apr. 09, 2023. [Online]. Available: https://www.chademo.com/about-us/what-is-chademo

[7] S. Aghajan-Eshkevari, S. Azad, M. Nazari-Heris, M. T. Ameli, and S. Asadi, "Charging and Discharging of Electric Vehicles in Power Systems: An Updated and Detailed Review of Methods, Control Structures, Objectives, and Optimization Methodologies," *Sustainability (Switzerland)*, vol. 14, no. 4. MDPI, Feb. 01, 2022. doi: 10.3390/su14042137.

[8] A. K. Seth and M. Singh, "Modified repetitive control design for two stage off board Electric Vehicle charger," *ISA Trans*, vol. 128, pp. 343-356, Sep. 2022, doi: 10.1016/j.isatra.2021.09.015.

[9] B. Lou, H. Zhou, S. Lu, C. Ying, W. Hua, and Z. Xu, "Extended control strategies of voltage source converter stations linked to converter dominated systems," *The Journal of Engineering*, vol. 2019, no. 16, pp. 1947-1951, Mar. 2019, doi: 10.1049/joe.2018.8719.

[10] IEEE Staff, *2018 IEEE Applied Power Electronics Conference and Exposition (APEC)*. IEEE, 2018.

[11] E. A. Al-Ammar, A. Ul-Haq, A. Iqbal, M. Jalal, and A. Anjum, "SRF based versatile control technique for DVR to mitigate voltage sag problem in distribution system," *Ain Shams Engineering Journal*, vol. 11, no. 1, pp. 99-108, Mar. 2020, doi: 10.1016/j.asej.2019.09.001.

[12] R. Kumar and B. Singh, "Grid Interactive Solar PV-Based Water Pumping Using BLDC Motor Drive," *IEEE Trans Ind Appl*, vol. 55, no. 5, pp. 5153-5165, Sep. 2019, doi: 10.1109/TIA.2019.2928286.

[13] B. Singh and S. Murshid, "A grid-interactive permanent-magnet synchronous motor-driven solar water-pumping system," *IEEE Trans Ind Appl*, vol. 54, no. 5, pp. 5549-5561, Sep. 2018, doi: 10.1109/TIA.2018.2860564.

[14] A. Verma and B. Singh, "Multi-Objective Reconfigurable Three-Phase Off-Board Charger for EV," in *IEEE Transactions on Industry Applications*, Institute of Electrical and Electronics Engineers Inc., Jul. 2019, pp. 4192-4203. doi: 10.1109/TIA.2019.2908950.

[15] S. H. Qazi, M. W. Mustafa, and S. Ali, "Review on Current Control Techniques of Grid Connected PWM-VSI Based Distributed Generation," *ECTI Transactions on Electrical Engineering, Electronics, and Communications*, vol. 17, no. 2, pp. 152-168, Aug. 2019, doi: 10.37936/ecti-eec.2019172.219187.

[16] J. K. Singh and R. K. Behera, "An Improved Hysteresis Current Controller for Grid-Connected Inverter System to Address Power Quality Issues at Reduced Switching Frequency," *IEEE Trans Ind Appl*, vol. 57, no. 2, pp. 1892-1901, Mar. 2021, doi: 10.1109/TIA.2021.3052426.

[17] S. Eberlein and K. Rudion, "Small-signal stability modelling, sensitivity analysis and optimization of droop controlled inverters in LV microgrids," *International Journal of Electrical Power and Energy Systems*, vol. 125, Feb. 2021, doi: 10.1016/j.ijepes.2020.106404.

[18] C. Balasundar, C. K. Sundarabalan, J. Sharma, N. S. Srinath, and J. M. Guerrero, "Design of power quality enhanced sustainable bidirectional electric vehicle charging station in distribution grid," *Sustain Cities Soc*, vol. 74, Nov. 2021, doi: 10.1016/j.scs.2021.103242.

[19] S. Kewat, B. Singh, and I. Hussain, "Power management in PV-battery-hydro based standalone microgrid," *IET Renewable Power Generation*, vol. 12, no. 4, pp. 391-398, Mar. 2018, doi: 10.1049/iet-rpg.2017.0566.

[20] IEEE Industry Applications Society. Static Power Converter Committee. and IEEE Power Engineering Society. Transmission and Distribution Committee., *IEEE recommended practices and requirements for harmonic control in electric power systems*. Institute of Electrical and Electronics Engineers, 1993.

[21] S. Habib, M. M. Khan, F. Abbas, L. Sang, M. U. Shahid, and H. Tang, "A Comprehensive Study of Implemented International Standards, Technical Challenges, Impacts and Prospects for Electric Vehicles," *IEEE Access*, vol. 6. Institute of Electrical and Electronics Engineers Inc., pp. 13866-13890, Mar. 05, 2018. doi: 10.1109/ACCESS.2018.2812303.

[22] G. Sharma, V. K. Sood, M. S. Alam, and S. M. Shariff, "Comparison of common DC and AC bus architectures for EV fast charging stations and impact on power quality," *eTransportation*, vol. 5, Aug. 2020, doi: 10.1016/j.etran.2020.100066.

[23] B. Dimitrov, K. Hayatleh, S. Barker, G. Collier, S. Sharkh, and A. Cruden, "A buck-boost transformerless DC-DC converter based on IGBT modules for fast charge of electric vehicles," *Electronics (Switzerland)*, vol. 9, no. 3, Mar. 2020, doi: 10.3390/electronics9030397.

[24] N. Zhou, J. Wang, Q. Wang, and N. Wei, "Measurement-Based Harmonic Modeling of an Electric Vehicle Charging Station Using a Three-Phase Uncontrolled Rectifier," *IEEE Trans Smart Grid*, vol. 6, no. 3, pp. 1332-1340, May 2015, doi: 10.1109/TSG.2014.2374675.


Received 13 November 2023